Crystal structure of the Chevrel phase $SnMo_6S_8$ at high pressure

L. Ehm* and P. Dera
Geophysical Laboratory, Carnegie Institution of Washington, 5251 Broad Branch Road N.W., Washington, D.C. 20015, USA

K. Knorr
Institut für Geowissenschaften, Mineralogie/Kristallographie, Christian-Albrechts-Universität zu Kiel, Olshausenstraße 40, 24098 Kiel, Germany

B. Winkler
Institut für Mineralogie, Abteilung Kristallographie, Johann Wolfgang Goethe-Universität, Senckenberganlage 30, 60054 Frankfurt am Main, Germany

A. Krimmel
Experimentalphysik V, Elektronische Korrelationen und Magnetismus, Institut für Physik, Universität Augsburg, 86135 Augsburg, Germany

P. Bouvier
ESRF, BP 220, F-38043, Grenoble Cedex 9, France
(Received 24 January 2005; published 14 July 2005)

The high-pressure behavior of the Chevrel phase $SnMo_6S_8$ was investigated by angular dispersive synchrotron powder diffraction. The experiments were accompanied by first principles calculations at the density functional theory level. The fit of a Birch-Murnaghan equation-of-state gave the volume at zero pressure $V_0=277(1)$ Å^3, the bulk modulus at zero pressure $B_0=84(3)$ GPa, and the pressure derivative of the bulk modulus $B'=3.0(4)$ for the experimental data and $V_0=281.6(3)$ Å^3, $B_0=76(1)$ GPa, and $B'=4.7(1)$ for the calculated data. The analysis of the bond distances and the bond population reveals the formation of new bonds and changes of the bond characteristics in the structure under pressure. The compression mechanism is analysed by means of the distortion of the Mo_6S_8 cluster and the rotation of the cluster with respect to the unit cell edges.

DOI: 10.1103/PhysRevB.72.014113 PACS number(s): 61.10.−i, 64.30.+t, 62.50.+p, 91.60.Gf

I. INTRODUCTION

The ternary molybdenum chalcogenides with the composition $M_xMo_6X_8$ (M=metals; X=S, Se, Te and $0 \leqslant x \leqslant 4$), also known as Chevrel-phases, have attracted considerable interest, due to high superconducting transition temperatures ($T_c \approx 14$ K), a remarkable high critical magnetic field ($H_{c2} \approx 60$ T), coexistence of magnetism and superconductivity,[1] possible applications as thermoelectric materials[2,3] and as cathode materials in rechargeable batteries.[4–7] Chevrel phases crystallize in the rhombohedral space-group $R\bar{3}$ or in a triclinic distorted form with the space-group $P\bar{1}$.[8–14] The structures consist of Mo_6X_8 clusters comprised of a distorted Mo_6 octahedron embedded in a deformed X_8 cube. The clusters form a pseudo-cubic array and are connected by the M atoms (Fig. 1). Chevrel phases with higher degrees of cluster condensations, e.g., Mo_9X_{11}, $Mo_{15}X_{17}$ or more than one cluster species were also reported.[9,15,16] $SnMo_6S_8$ crystallizes in the space group $R\bar{3}$ (SG Int. Tab. 148) with the lattice parameters $a=6.527(1)$ Å and $\alpha=89.7(1)°$. The tin atom is located on the Wyckoff position $1a$ (0, 0, 0), sulfur [S(2)] on $2c$ (x,x,x) with $x=0.241\,2(3)$, molybdenum and sulfur [S(1)] on $6f$ (x,y,z) with $x=0.225\,09(8)$, $y=0.416\,32(8)$, $z=0.561\,09(8)$ for molybdenum and $x=0.379\,4(3)$, $y=0.125\,9(3)$, $z=0.743\,6(4)$ for sulfur, respectively.[17]

The magnetic and electronic properties of Chevrel phases with different metals on the M position were comprehensively studied experimentally and theoretically.[1,18–21] The metal atom in the Chevrel phase defines the magnetic behavior, whereas the superconducting properties are mostly determined by the electronic structure of the Mo_6X_8 cluster. Oxygen defects in the sulfur sublattice of the Chevrel phases have been found to decrease the superconduction temperature T_c and increase in the upper critical field H_{c2}.[22–26] Lattice dynamics calculations in combination with Raman spectroscopic measurements on Chevrel phases with various metal atoms revealed that the Raman active phonons are independent of the particular metal atom.[27–29]

Structural phase transitions at low temperatures in rhombohedral Chevrel phases with different composition were observed by x-ray diffraction.[30–33] The rhombohedral structure of the Chevrel phases distorts slightly into triclinic symmetry. The temperature dependence of the elastic constants was studied by Wolf *et al.*[34] using ultrasonic techniques. The investigations of the high-pressure behavior of Chevrel phases was focussed on their electronic properties. Shelton *et al.*,[35] Capone *et al.*,[24] and Yao *et al.*[36] studied the pressure dependence of T_c in $SnMo_6S_8$ up to 2.2 GPa, 1.2 GPa, and 10 GPa, respectively. They found a decrease of the transition temperature T_c with a minimum of 4 K at 9 GPa. The influence of pressure on the transition temperature of the structural phase transition and T_c in $EuMo_6S_8$ has been studied by

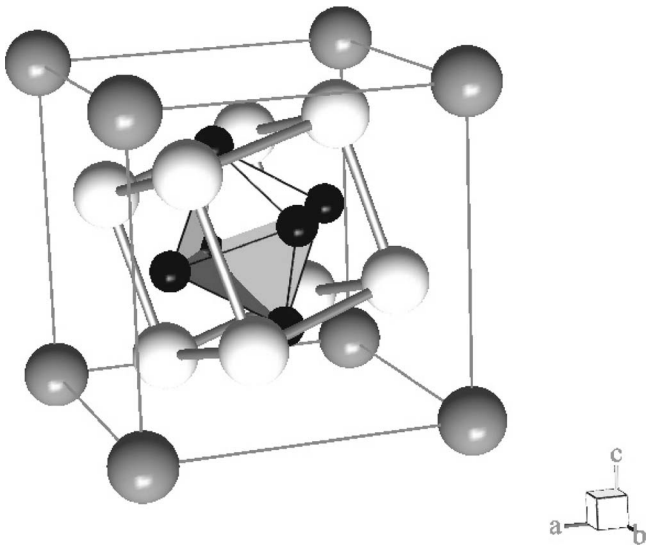

FIG. 1. Crystal structure of the Chevrel phase $SnMo_6S_8$. The dark gray spheres represent tin atoms, the black spheres molybdenum atoms, and the light gray spheres, sulfur atoms. The octahedron formed by the molybdenum atoms is plotted in light gray.

Decroux *et al.*[37] and Capone *et al.*[23] They found a dramatic drop of the transition temperature from 109 K at ambient pressure to 0 K at 1.32 GPa. Furthermore, they observed a sharp superconducting transition at 1.32 GPa and 12.2 K. Compressibility measurements on eleven Chevrel phases were performed by Webb and Shelton[38] employing the piston displacement technique. However, neither experimental nor theoretical investigations of the pressure dependence of the structure of Chevrel phases are reported in literature.

Here the results of a high-pressure study of the crystal structure of $SnMo_6S_8$ up to a pressure of 38 GPa, performed jointly by synchrotron powder diffraction and density functional theory (DFT) calculation, are presented.

II. METHODS

A. Experimental details

$SnMo_6S_8$ was crystallized from the elements by high temperature synthesis. A stoichiometric mixture of tin, molybdenum, and sulfur was sealed in an evacuated silica tube and kept for 4 days at 1273 K and then gradually cooled to room temperature. The reaction product was analyzed using conventional x-ray powder diffraction and the stoichiometry of the sample was verified by electron microprobe analysis using a Cameca Camebax microprobe. The results confirm that the product is a single phase, and of ideal composition within the range of experimental errors. The high-pressure diffraction experiments up to 38 GPa were performed at the beamline ID30 at the ESRF in Grenoble, France. High-pressure powder diffraction patterns were collected at a wavelength of $\lambda = 0.3738$ Å using a MarResearch (mar345) image plate detector with a pixel-size of 100×100 μm^2. The incident beam was focused to 30×30 μm^2 at the sample position. A grid of 3×3 points on the specimen was sampled with the x-ray beam for 4 s, giving a total exposure time of 36 s per image. Pressure was applied using a membrane driven diamond anvil cell. The sample was placed in the hole ($d = 200$ μm) of an Inconel gasket preindented to 80 μm. In order to ensure quasihydrostatic conditions nitrogen was used as pressure transmitting medium. The ruby fluorescence method was used for pressure determination applying the Mao pressure scale.[39] A silicon standard placed at the sample position was used to determine the sample to detector distance. Geometry parameters for the radial integration of the two-dimensional data were determined using FIT2D.[40] For the transformation into standard one-dimensional powder patterns the software TWO2ONE (Refs. 41 and 42) was used.

Lattice parameters were obtained from whole-powder-pattern refinement and the structure was refined by the Rietveld method employing the program FULLPROF.[43] The background was described by a fourth order polynomial and the peak profiles were modelled using a modified pseudo-Voigt function.[44] Seven structural parameters were refined, the fractional coordinates (x, y, z) for Mo and S(1) and the coordinate x for S(2), respectively. The standard deviations of the refined parameters were scaled with the Bérar-factor.[45] The pressure-volume data were fitted by a third-order Birch-Murnaghan equation-of-state [Eq. (1)],[46]

$$p(V) = \frac{3}{2} B_0 \left[\left(\frac{V}{V_0} \right)^{-(7/3)} - \left(\frac{V}{V_0} \right)^{-(5/3)} \right] \times \left(1 + \frac{3}{4} (B' - 4) \left[\left(\frac{V}{V_0} \right)^{-(2/3)} - 1 \right] \right). \quad (1)$$

B. Computational details

The quantum mechanical calculations described here are based on density functional theory. In these calculations the Perdew-Burke-Ernzerhof-version of the generalized gradient approximation (GGA) was employed.[47] For these calculations we used academic and commercial versions of the CASTEP program, which has been described elsewhere.[48–50] In these calculations, ultrasoft pseudopotentials were used with a maximum cutoff energy of the plane waves of 320 eV. In addition to the cutoff energy, one further parameter determines the quality of the calculations, namely the density of points with which the Brillouin zone is sampled. The wave vectors for the sampling points were chosen according to the scheme proposed by Monkhorst and Pack.[51] Here, we use a sampling of the reciprocal space such that distances between grid points are less than 0.04 $Å^{-1}$. All structural parameters not constrained by the space group symmetry have been relaxed for given pressures using a standard BFGS-algorithm based on a Hessian in the mixed space of cell parameters and internal degree of freedom. After the final self-consistency cycle the remaining stress was less than 0.02 GPa. The present calculations are restricted to the athermal limit, in which temperature effects and zero-point motions are neglected.

III. RESULTS AND DISCUSSION

X-ray powder diffraction patterns were collected from ambient pressure up to 38.2(7) GPa. Figure 2 shows ob-

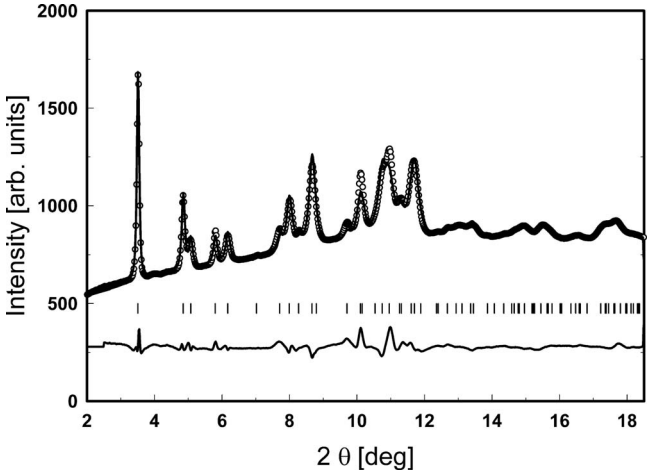

FIG. 2. Observed (circles) and calculated (solid line) diffraction pattern for $SnMo_6S_8$ at 21.7(6) GPa (R_p: 11.0, R_{wp}: 11.6, χ^2: 1.77). At the bottom of the figure the difference and the tick marks for the calculated reflection positions are plotted.

served and calculated diffraction patterns of $SnMo_6S_8$ at 21.7(6) GPa and demonstrates the high quality of the diffraction data.

The structure of $SnMo_6S_8$ could be refined in the space group $R\bar{3}$ up to the highest pressure of 38.2(7) GPa.

The total and the partial densities of states of $SnMo_6S_8$ at ambient pressure are presented in Fig. 3. For these calculation, a $4\times4\times4$ Monkhorst-Pack grid in conjunction with a linear interpolation scheme was employed. The partial densities of states were obtained from the Mulliken population analysis.

The evolution of the measured and computed lattice parameters a and α with pressure is shown in Fig. 4. The pressure dependence of the measured and calculated normalized unit cell volume is presented in Fig. 5.

The unit cell volume at zero pressure V_0, the bulk modulus B_0 and the pressure derivative of the bulk modulus B' $=\partial B_0/\partial p$ were derived from fits of a third-order Birch-Murnaghan equation-of-state to the experimentally determined and calculated volume data. The results of the fits are given in Table I.

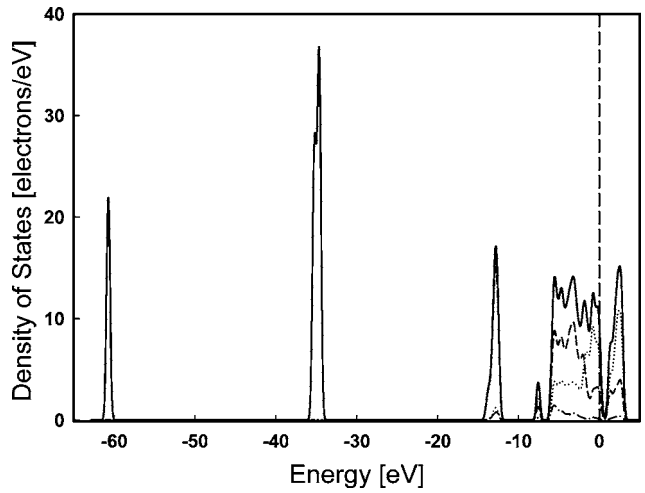

FIG. 3. Calculated density of states for $SnMo_6S_8$. The partial density of states for the s-band (dashed-dotted), p-band (dashed), and d-band (dotted) are plotted. The total density of states is shown as a solid line. The vertical dashed line represents the Fermi energy.

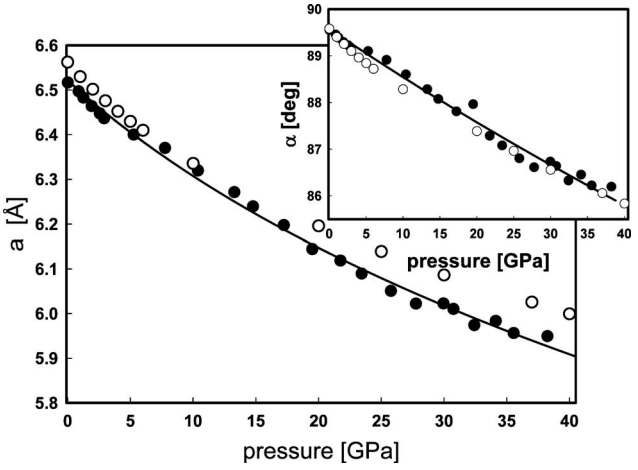

FIG. 4. Pressure dependence of the lattice parameters of $SnMo_6S_8$. The solid symbols represent the experimentally determined data and the open symbols the data points obtained from *ab initio* calculations. The experimental error bars for the pressure and the lattice parameters correspond to the size of the symbols. The lines are fits of a third-order Birch-Murnaghan equation-of-state to the experimental data.

The volume at zero pressure as well as the bulk modulus B_0 show a good agreement between experimental and calculated values, whereas the pressure derivative B' differs. DFT-GGA calculations generally give too large unit cell parameters in comparsion to experimentally determined values. This is due to the well-established "underbinding," and leads to deviations of 1%–2% for the cell parameters. Consequently, bulk moduli obtained from DFT-GGA calculations

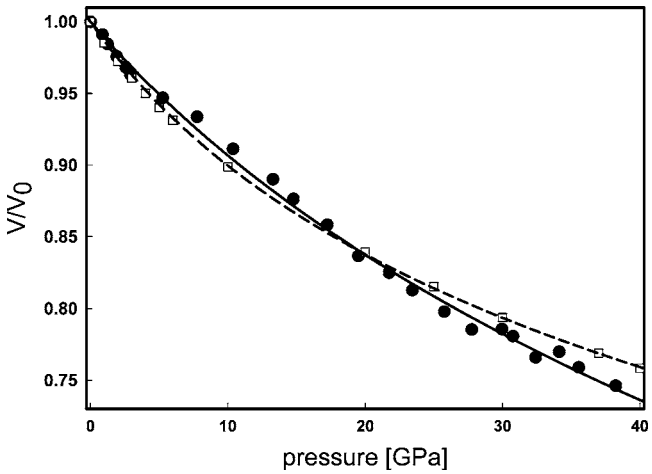

FIG. 5. Pressure dependence of the normalized unit cell volume of $SnMo_6S_8$. The solid symbols represent the experimentally determined data and the open symbols are the data points derived from *ab initio* calculations. The experimental error bars for the pressure and the normalized volume correspond to the size of the symbols. The lines are fits of a third-order Birch-Murnaghan equation-of-state to the experimental (solid) and calculated (dashed) data.

TABLE I. Results of a fit of a third-order Birch-Murnaghan equation-of-state to the experimental and calculated data points. The values for the bulk modulus of $Sn_{1.2}Mo_6S_8$ and its pressure derivative reported by Webb and Shelton (Ref. 38) are given as well.

	V_0 (Å^3)	B_0 (GPa)	B'
exp.	277(1)	84(3)	3.0(4)
calc.	281.6(3)	76(1)	4.7(1)
lit.		35.44	3.55

are generally too small by a few GPa. These general findings are confirmed here, and the satisfactory agreement between theory and experiment then allows us to evaluate the theoretical data further. The difference in B' probably arises from the quasihydrostatic conditions generated by the N_2 pressure medium above 20 GPa in the powder diffraction experiment. The bulk modulus of 35.44 GPa for $Sn_{1.2}Mo_6S_8$ reported by Webb and Shelton[38] differs significantly from the experimental and calculated values derived in this work. However, the difference can be attributed to the limited pressure range of 3 GPa and large measurement uncertainties of the piston displacement in the work of Webb and Shelton.[38]

The experimentally determined bond distances for selected pressures are presented in Table II. The bond distances determined at ambient conditions are in an excellent accordance with the calculated values and distances given in literature.[17] The changes in the fractional coordinates over the entire pressure range are small. The individual bonds in $SnMo_6S_8$ show a different compression behavior. The Mo—Mo distances in the Mo_6S_8 cluster at ambient conditions are 2.732(2) Å and 2.659(5) Å and therefore close to the Mo—Mo distance of 2.725 Å observed in pure molydenum.[52] At a pressure of 38.2(7) GPa the Mo—Mo distance decreased by 1.77% and 6.78%, respectively. In the *ab initio* calculations a similar decrease of the Mo—Mo distances of 1.54% and 3.93% was observed at a pressure of 40 GPa. The four Mo—S bond distance in the cluster at ambient conditions are Mo—S(1) 2.442(2) Å, Mo—S(1) 2.442(2) Å, Mo—S(1) 2.496(8) Å, and Mo—S(2) 2.41(2) Å, respectively. The values are slightly smaller than the expected value of 2.58 Å calculated from the effective ionic radii.[53] The Mo—S bond distances are reduced by 6.90%, 7.70%, 3.65%, and 2.13% at a pressure of 38.2(7) GPa. A decrease of the Mo—S distances of 3.82%, 5.67%, 1.33%, and 3.08% was determined from the quantum mechanical calculations at 40 GPa. Two different S—S distances with S(1)—S(1) 3.39(1) Å and S(1)—S(2) 3.50(1) Å are realized at ambient pressure. The S—S distances decreased by 9.45% and 1% at a pressure of 38.2(7) GPa in the experiment and by 6.68% and 0.46% at a pressure of 40 GPa in the calculations. The experimental values for the Sn—S distances at room pressure are 3.091(4) Å for Sn—S(1) and 2.705(1) Å for Sn—S(2). Both distances are signifficantely larger than the value of 2.44 Å calculated from the ionic radii.[53] The Sn—S(1) distance is too long to be considered as a bond at ambient pressure. However, at 38.2(7) GPa the distance reduced by 16.5% to 2.58(1) Å and a formation of a bond between Sn and S(2) seems probable. The Sn—S(2) bond is less compressible and decreased by 8.37% at a pressure of 38.2(7) GPa. The quantum mechanical calculations reveal a reduction of 23.99% for the Sn—S(1) and 4.12% for the Sn—S(2) bond distance at 40 GPa. Remarkably, the longer Mo—Mo distance and the long S—S distance are less compressible than the shorter once.

The quantum mechanical calculations allow an extensive analysis of the pressure induced changes of the bonds, by evaluation of the bond population. The bond population is uneffected by pressure for the Mo—Mo bonds and most of the Mo—S bonds. However, a reduction from 0.19 *e* to 0.05 *e* was observed for one Mo—S(1) bond with increasing pressure. The bond population analysis of the Sn—S bonds confirms the interpretation from the bond distance analysis, that a bond between Sn and S(1) is formed under pressure. The bond forms at a pressure of 25 GPa and is further populated with pressure to 0.05 *e* at 40 GPa. The decrease in the bond population of the Mo—S(1) bond is a direct result of the newly-formed Sn—S(1) bond. In order to form the bond with the tin atom, electrons of the sulfur are transferred from the Mo—S(1) bond towards the newly formed Sn—S(1) bond. The Sn—S(2) bond population is very sensitive to pressure as well; it increases form 0.21 *e* at ambient pressure

TABLE II. Experimentally determined bond distances in Å at selected pressures.

p (GPa)	0.01	2.90(1)	10.3(3)	14.7(4)	21.7(6)	27.7(5)	34.1(5)	38.2(7)
Sn—S(1)	3.091(4)	2.999(3)	2.778(2)	2.761(6)	2.689(5)	2.647(4)	2.640(3)	2.580(9)
Sn—S(2)	2.705(1)	2.713(9)	2.599(6)	2.616(6)	2.607(5)	2.570(3)	2.553(4)	2.478(6)
Mo—Mo	2.732(2)	2.718(5)	2.660(7)	2.672(8)	2.669(6)	2.676(5)	2.672(6)	2.683(8)
Mo—Mo	2.659(5)	2.697(8)	2.634(6)	2.604(3)	2.558(7)	2.482(6)	2.478(7)	2.479(9)
Mo—S(1)	2.442(2)	2.453(5)	2.492(4)	2.439(7)	2.378(5)	2.295(7)	2.269(4)	2.273(8)
Mo—S(1)	2.442(2)	2.369(3)	2.330(5)	2.333(6)	2.379(7)	2.349(7)	2.325(7)	2.254(6)
Mo—S(1)	2.496(8)	2.539(3)	2.602(3)	2.542(5)	2.506(4)	2.450(5)	2.436(6)	2.405(7)
Mo—S(2)	2.41(2)	2.40(4)	2.444(6)	2.392(4)	2.346(9)	2.312(7)	2.308(6)	2.354(9)
S(1)—S(1)	3.39(1)	3.44(2)	3.49(1)	3.39(2)	3.28(2)	3.12(3)	3.09(2)	3.07(2)
S(1)—S(2)	3.50(1)	3.43(9)	3.47(1)	3.45(2)	3.48(1)	3.50(2)	3.49(2)	3.46(2)

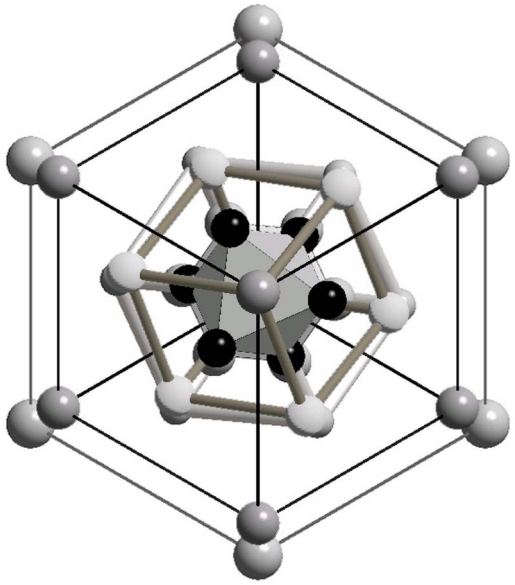

FIG. 6. (Color online) Projection of the Chevrel structure along the [111] direction. The structure at ambient conditions is overlayed by the structure at 25.7(4) GPa, showing the anticlockwise rotation by 5° of the Mo_6S_8-cluster about the [111]-axis.

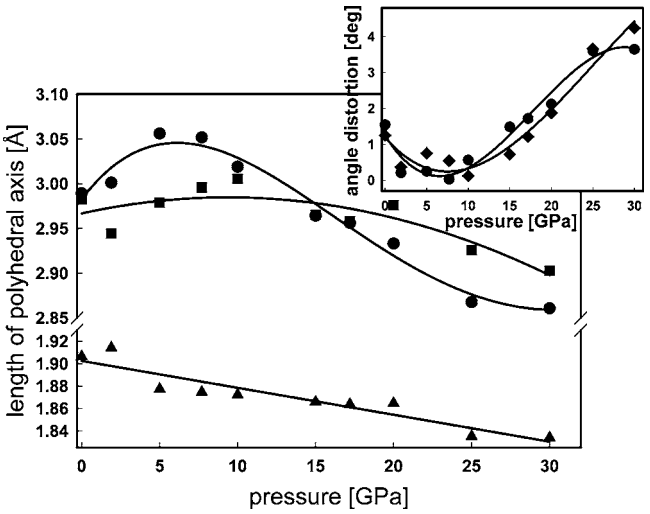

FIG. 7. Evolution of the distances from the center of the polyhedra to the Mo (triangle), S(1) (circle), and S(2) (square) atoms. The inset shows the deviation of the angles in the real Mo_6 (circle) and S_8 (diamond) polyhedra from the angles in their ideal representations with pressure. The lines are guides for the eyes.

to 0.39 *e* at 40 GPa. While a Mulliken bond population analysis is a qualitative indicator only, the calculated changes clearly show an increased interaction between the tin atom on the *M* position and the cluster with pressure.

Furthermore, the geometrical aspects of the compression mechanism can be evaluated from the analysis of the Mo_6S_8 cluster. The idealized geometry of the cluster corresponds to a Mo_6 octahedron enbedded within a S_8 cube. The form is a tetracishexaeder, characterized by equal distances from all the atoms to the center of mass. However, the center-molybdenum distances are smaller than the corresponding center-sulfur distances in the real structure. Therefore, the cluster is better described as a sulfur cube having molybdenum atoms almost at the centers of the cube faces. The cube is slightly distorted due to the rhombohedral space group symmetry, such that the sulfur atoms form a rhombohedron and the molydenum atoms a trigonal antiprism.

The compression mechanism can be decomposed into the distortion of the cluster and the rotation of the cluster with respect to the unit cell edges. The cluster is rotated around the rhombohedral axis about 5° at 25 GPa (Fig. 6).

The rotation leads to a shortening of the Sn—S(1) distance and governs the formation of the new Sn—S(1) bond, as discussed above. The deformation of the cluster can be further decomposed into length and angular distortions of the two different coordination polyhedra. Figure 7shows the variations of the polyhedral axis length with pressure. Whereas, the center-molybdenum distances change linearly, the center-sulfur distances behave diffferently.

The center-sulfur distance parallel to the $\bar{3}$ axis are almost constant with increasing pressure, while the remaining distances increase up to a pressure of 5 GPa before they decrease continuously. Notable is the crossover at about 12 GPa, which corresponds to a transition from a compressed to an elongated rhombohedron. The angular distortion in the Mo_6S_8 cluster is quantified by the deviation of the angles in the real Mo_6 and S_8 polyhedra from the angles in their ideal representations (90° for the octahedron and 109.47° for the cube). Both polyhedra show similar angular distortion behavior with pressure (inset Fig. 7). The minimum for the S_8 distortion curve coincides with crossover point in axis of the sulfur rhombohedron, i.e., the rhombohedron distorts towards a cube, before a further deformation occurs at pressure higher than 12 GPa.

IV. SUMMARY

The high-pressure behavior of the Chevrel phase $SnMo_6S_8$ was studied by x-ray powder diffraction and quantum mechanical calculations up to 38.2(7) GPa. The bulk moduli and their pressure derivatives were determined from the experimental data and the results of the first principles calculations. The compression mechanism was described by means of angle and length distortions of the axis of the coordination polyhedra and the rotation of the Mo_6S_8 cluster with respect to the unit cell edges. The analysis of the bond distances and the bond population revealed the formation of a new bond between the sulfur and tin atoms and an increasing interaction of the cluster and the *M* atoms with pressure.

ACKNOWLEDGMENTS

L.E., K.K., and A.K. would like to thank the European Union for support under the TMR program. L.E. is grateful to the German Science Foundation (DFG) for funding under Grants Nos. De 412/21-1 and FOR 345/1-1, and the support through a Postdoctoral Fellowship of the Carnegie Institution

of Washington. L.E. and P.D. are grateful to the National Science Foundation (NSF) for support under Grant No. NSF EAR-0217389. Furthermore, we are grateful for computer time provided by the Center for Scientific Computation of the University of Frankfurt am Main. Additional computer time was kindly made available by HP. Software was generously provided by Accelrys and the CASTEP developers group.

*Electronic address: l.ehm@gl.ciw.edu

[1] O. Fischer, Appl. Phys. **16**, 1 (1978).
[2] C. Roche, P. Pecheur, T. Toussaint, A. Jenny, H. Scherrer, and S. Scherrer, J. Phys.: Condens. Matter **10**, L333 (1998).
[3] R. W. Nunes, I. I. Mazin, and D. J. Singh, Phys. Rev. B **59**, 7969 (1999).
[4] S. T. Coleman, W. R. McKinnon, and J. R. Dahn, Phys. Rev. B **29**, 4147 (1984).
[5] C. Ritter, E. Gocke, C. Fischer, and R. Schöllhorn, Mater. Res. Bull. **27**, 1217 (1992).
[6] E. Lancry, E. Levi, Y. Gofer, M. Levi, G. Salitra, and D. Aurbach, Chem. Mater. **16**, 2832 (2004).
[7] E. Levi, Y. Gofer, Y. Vestfreed, E. Lancry, and D. Aurbach, Chem. Mater. **14**, 2767 (2002).
[8] R. Chevrel, M. Sergent, and J. Prigent, J. Solid State Chem. **3**, 515 (1971).
[9] R. Chevrel, M. Sergent, B. Seeber, and O. Fischer, Mater. Res. Bull. **14**, 567 (1979).
[10] L. L. Lay, D. R. Powell, and T. C. Willis, Acta Crystallogr., Sect. C: Cryst. Struct. Commun. **C48**, 1179 (1992).
[11] C. Roche, R. Chevrel, A. Jenny, P. Pecheur, H. Scherrer, and S. Scherrer, Phys. Rev. B **60**, 16442 (1999).
[12] F. Le Berre, C. Hamard, O. Peña, and A. Wojakowski, Inorg. Chem. **39**, 1100 (2000).
[13] S. Belin, R. Chevrel, and M. Sergent, J. Solid State Chem. **145**, 159 (1999).
[14] S. Belin, R. Chevrel, and M. Sergent, J. Solid State Chem. **155**, 250 (2000).
[15] G. Grüttner, K. Yvon, R. Chevrel, M. Potel, M. Sergent, and B. Seeber, Acta Crystallogr., Sect. B: Struct. Crystallogr. Cryst. Chem. **B35**, 285 (1979).
[16] P. Gougeon, M. Potel, and M. Sergent, Acta Crystallogr., Sect. C: Cryst. Struct. Commun. **C45**, 182 (1989).
[17] R. Chevrel, C. Rossel, and M. Sergent, J. Less-Common Met. **72**, 31 (1980).
[18] F. C. Brown, B. A. Bunker, D. M. Ginsberg, T. J. Miller, W. M. Miller, and E. A. Stern, Phys. Rev. B **34**, 7698 (1986).
[19] D. N. Zheng, H. D. Ramsbottom, and D. P. Hampshire, Phys. Rev. B **52**, 12931 (1995).
[20] J. Tobola, P. Pecheur, H. Scherrer, S. Kaprzyk, Y. Ohta, and Y. Matsumura, J. Phys.: Condens. Matter **15**, L655 (2003).
[21] H. J. Niu and D. P. Hampshire, Phys. Rev. B **69**, 174503 (2004).
[22] D. G. Hinks, J. D. Jorgensen, and H. C. Li, Phys. Rev. Lett. **51**, 1911 (1983).
[23] D. W. Capone, II, R. P. Guertin, S. Foner, D. G. Hinks, and H. C. Li, Phys. Rev. Lett. **51**, 601 (1983).
[24] D. W. Capone, II, R. P. Guertin, S. Foner, D. G. Hinks, and H. C. Li, Phys. Rev. B **29**, R6375 (1984).
[25] S. Foner, E. J. McNiff, Jr., and D. G. Hinks, Phys. Rev. B **31**, R6108 (1985).
[26] C. L. Chang, Y. K. Tao, J. S. Swinnea, and H. Steinfink, Acta Crystallogr., Sect. C: Cryst. Struct. Commun. **C43**, 1461 (1987).
[27] S. D. Bader and S. K. Sinha, Phys. Rev. B **18**, 3082 (1978).
[28] D. J. Holmgren, R. T. Demers, M. V. Klein, and D. M. Ginsberg, Phys. Rev. B **36**, 5572 (1987).
[29] D. J. Holmgren, R. T. Demers, M. V. Klein, and D. M. Ginsberg, Phys. Rev. B **36**, 1952 (1987).
[30] R. Baillif, A. Dunand, J. Muller, and K. Yvon, Phys. Rev. Lett. **47**, 672 (1981).
[31] F. Kurbel and K. Yvon, Acta Crystallogr., Sect. C: Cryst. Struct. Commun. **C43**, 1655 (1987).
[32] F. Kurbel and K. Yvon, Acta Crystallogr., Sect. C: Cryst. Struct. Commun. **C46**, 181 (1990).
[33] M. Francois, K. Yvon, D. Cattani, M. Decroux, R. Chevrel, M. Sergent, S. Boudjada, and T. Wroblewski, J. Appl. Phys. **75**, 423 (1994).
[34] B. Wolf, J. Molter, G. Bruls, B. Lüthi, and L. Jansen, Phys. Rev. B **54**, 348 (1996).
[35] R. N. Shelton, A. C. Lawson, and D. C. Johnston, Mater. Res. Bull. **10**, 297 (1975).
[36] Y. S. Yao, R. P. Guertin, D. G. Hinks, J. Jorgensen, and D. W. Capone, II, Phys. Rev. B **37**, 5032 (1988).
[37] M. Decroux, M. S. Torikachvili, M. B. Maple, R. Baillif, O. Fischer, and J. Muller, Phys. Rev. B **28**, 6270 (1983).
[38] A. W. Webb and R. N. Shelton, J. Phys. F: Met. Phys. **8**, 261 (1978).
[39] H. K. Mao, P. M. Bell, J. W. Shaner, and D. J. Steinberg, J. Appl. Phys. **49**, 3276 (1978).
[40] A. Hammersley, S. Svensson, M. Hanfland, A. Fitch, and D. Häusermann, High Press. Res. **14**, 235 (1996).
[41] M. Chall, K. Knorr, L. Ehm, and W. Depmeier, High Press. Res. **17**, 315 (2000).
[42] S. Vogel, L. Ehm, K. Knorr, and G. Braun, Adv. X-Ray Anal. **45**, 31 (2002).
[43] J. Rodriguez-Carvajal, Physica B **192**, 55 (1993).
[44] P. Thompson, D. E. Cox, and J. B. Hastings, J. Appl. Crystallogr. **20**, 79 (1987).
[45] J.-F. Bérar, and P. Lelann, J. Appl. Crystallogr. **24**, 1 (1991).
[46] F. Birch, J. Geophys. Res. **83**, 1257 (1978).
[47] J. P. Perdew, K. Burke, and M. Ernzerhof, Phys. Rev. Lett. **77**, 3865 (1996).
[48] M. C. Payne, M. P. Teter, D. C. Allan, T. A. Arias, and J. D. Joannopoulos, Rev. Mod. Phys. **64**, 1045 (1992).
[49] M. D. Segall, P. L. D. Lindan, M. J. Probert, C. J. Pickard, P. J. Hasnip, S. J. Clark, and M. C. Payne, J. Phys.: Condens. Matter **14**, 2717 (2002).
[50] V. Milman, B. Winkler, J. A. White, C. J. Pickard, and M. C. Payne, Int. J. Quantum Chem. **77**, 895 (2000).
[51] H. J. Monkhorst and J. D. Pack, Phys. Rev. B **13**, 5188 (1976).
[52] A. W. Hull, Phys. Rev. **17**, 571 (1921).
[53] R. Shannon, Acta Crystallogr., Sect. A: Cryst. Phys., Diffr., Theor. Gen. Crystallogr. **32**, 751 (1976).